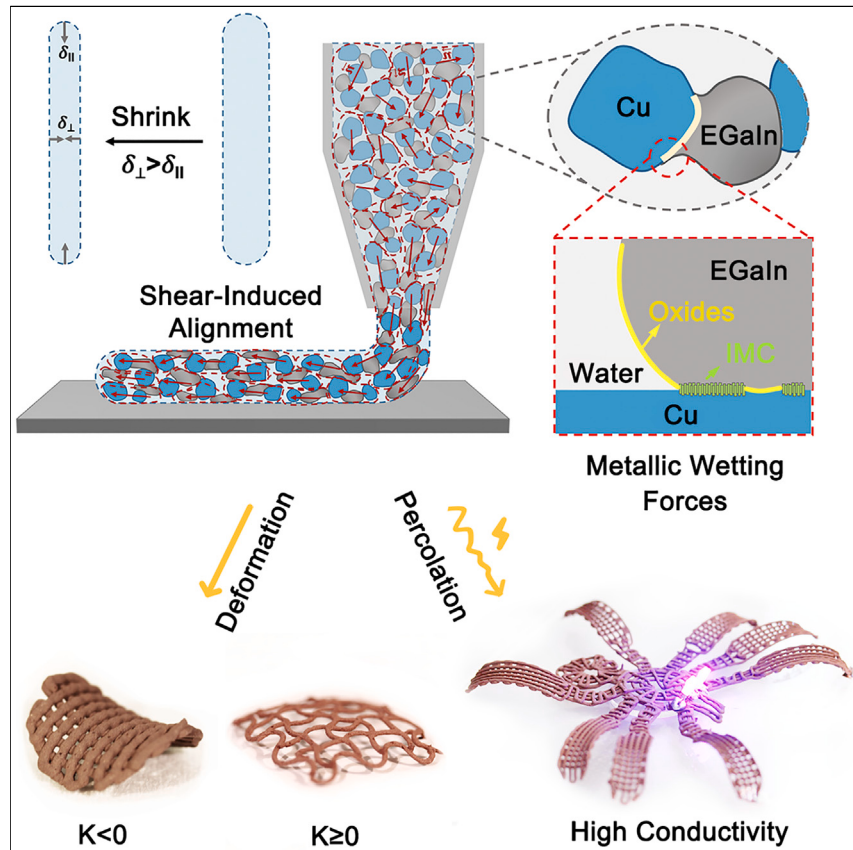


Article

Metallic gels for conductive 3D and 4D printing



Liquid metal (EGaIn) particles bridge copper particles suspended in water to create a metallic gel with rheological properties ideal for printing at room temperature. Shear from the nozzle aligns the particles to form structural anisotropy, enabling 4D printing by way of the stresses that arise during drying. The printed parts have metallic conductivity (1.05×10^5 S/m) without requiring a sintering step. Such conductive inks are promising for printing metallic structures under ambient conditions.

Ruijie Xing, Jiayi Yang,
Dongguang Zhang, ..., Jie Kong,
Wei Qi, Michael D. Dickey

tjuhrl@tju.edu.cn (R.H.)
qiwei@tju.edu.cn (W.Q.)
mddickey@ncsu.edu (M.D.D.)

Highlights

Metallic gels consisting of pendular suspension of Cu, EGaIn, and water

The gels are 3D-printable at room temperature over a wide compositional window

Shear alignment by dispensing enables 4D printing of conductive metal composites

Printed parts have metallic conductivity of 1.05×10^5 S/m without a sintering step

4

Demonstrate

Proof-of-concept of performance with intended application/response

Xing et al., Matter 6, 2248–2262
July 5, 2023 © 2023 Elsevier Inc.
<https://doi.org/10.1016/j.matt.2023.06.015>



Article

Metallic gels for conductive 3D and 4D printing

Ruizhe Xing,^{1,2,3} Jiayi Yang,^{1,4} Dongguang Zhang,^{1,5} Wei Gong,^{1,7} Taylor V. Neumann,¹ Meixiang Wang,¹ Renliang Huang,^{6,*} Jie Kong,² Wei Qi,^{3,*} and Michael D. Dickey^{1,8,*}

SUMMARY

This paper reports printable metallic gels (pendular suspensions) consisting of an aqueous suspension of copper particles connected by bridges of liquid eutectic gallium indium alloy (EGaIn). Pendular suspensions rely on capillary forces to form networks between solid particles with a composition-dependent rheology, but prior studies have focused on insulating suspensions. Here, the rheology of a conductive solid-liquid-liquid suspension is tuned for 3D printing by varying the composition and the pH; the latter promotes metallic wetting. The dry printed parts have metallic electrical conductivity (1.05×10^5 S/m) without requiring a sintering step. Drying at elevated temperatures can accelerate the removal of water while creating stress that drives shape change (i.e., 4D printing). As a demonstration, we print a conductive spider that lifts and assembles its own body from an initially flat shape. Such conductive inks are promising for printing metallic structures under ambient conditions.

INTRODUCTION

This paper reports a conductive, printable, and heat-responsive ink consisting primarily of copper (Cu) particles wetted by "bridges" of liquid metal in an aqueous solution. In general, wetting forces play an important role in stabilizing multiphase systems. For example, wetting between liquids and solid particles can strengthen wet granular materials,¹ stabilize foams² and binary liquids,³ or form "bijels."⁴ The attractive feature in these systems is that wetting offers a simple route to bind both solid and liquid particles together to form a new bulk material with tunable rheological properties (e.g., an increase of viscosity or yield stress), hence offering new processing routes for traditional granular materials.⁵

This work focuses on solid-liquid-liquid (S-L-L) "inks" stabilized by wetting forces. Previously, researchers have primarily focused on solid particles, such as silica or alumina, in mixtures of liquids, such as oil and water.⁶ The resulting morphology and rheology depend strongly on the relative amount of S-L-L as well as the relative wetting of the two immiscible liquids to the particles. One of the most fascinating morphologies is the pendular state, which is a gel that forms by adding a small amount of an immiscible liquid to a suspension of solid particles. If the additional liquid preferentially wets the particles, it can form thin liquid bridges between particles that stabilize elastic, gel-like networks of particles.⁷ This morphology is interesting because small additions of liquid can convert an S-L particle suspension into an S-L-L gel with rheological properties useful for printing. By varying the composition, it is possible to form inks with a range of different rheological properties, including those that can be direct-write or 3D printed.

Therefore, we reasoned that an S-L-L multiphase system consisting of solid Cu particles wetted by bridges of liquid metal (eutectic gallium indium, EGaIn) in the

PROGRESS AND POTENTIAL

Four-dimensional (4D) printing refers to 3D-printed structures that change shape with respect to time in response to an external stimulus. To date, 4D printing techniques have focused primarily on electrically insulating materials such as polymers. Adding conductive fillers to polymers could increase the functionality of the printed parts, but the high loadings necessary to achieve conductivity represent a trade-off with printability. Here, we connect copper (Cu) particles with soft eutectic gallium indium alloy (EGaIn) bridges to form a conductive 4D printing ink (Cu-EGaIn) with gel-like properties that are well suited for printing. The final printed parts have a total metal content as high as 97.5 wt %, and the remainder is methylcellulose, a rheological modifier. The printed parts have an extremely high electrical conductivity (1.05×10^5 S/m) without requiring a sintering step. Cu-EGaIn addresses the contradiction between conductivity and printability and should open up new opportunities for electronic, thermal, and composite devices.



presence of water should have high electrical conductivity yet also preserve suitable rheological properties to be extruded from a nozzle. Normally, extruding particle-loaded composites is challenging because of the rheology associated with the high loading necessary to ensure the particles percolate to form a conductive pathway.⁸ For example, consider a simple system of Cu microparticles in water. The Cu particles are prone to settle in the water because of gravity and undergo granular jamming when pushed through a nozzle; even if they could be printed, they may not preserve their shape upon exiting the nozzle and additional steps, such as heating, are necessary to sinter the particles into a conductive network. In contrast, by adding a small amount of liquid metal to the same suspension of Cu particles in water, it is possible to form conductive bridges between solid particles while imparting desirable rheological properties for printing.

Liquid metals have been printed previously in bulk⁹ as pastes (consisting of particles blended into bulk liquid metal)¹⁰ or as composites (consisting of liquid metal blended into a polymer).¹¹ Relative to those approaches, the approach here (1) uses less of the expensive liquid metal, (2) provides a wider range of tunable rheological properties, (3) ultimately creates solid rather than liquid parts, and (4) forms highly conductive parts without any special post-printing step to achieve conductivity.

To create the ink, we mixed EGaIn and Cu particles in the presence of water with a small amount of methylcellulose (MC) for rheological modification to assist with printing. Liquid metals have intrinsic metallic conductivity, low viscosity (similar to water), and effectively zero vapor pressure at room temperature.¹² EGaIn also wets most metals at room temperature, which is important for creating liquid bridges between Cu particles.¹³ To promote such metallic wetting, we temporarily removed native oxides by including some acid (HCl at pH 1) in the formulation, which ultimately evaporates after printing. Similar to prior S-L-L systems, we found several distinct morphologies that form depending on the relative amount of liquid metal, water, and Cu. Although not all compositions can be printed, there is a broad window of compositions that can form highly conductive structures at room temperature. Sintering is usually required to cause metallic inks to be rendered conductive. In the case of inks containing liquid metal particles, sintering has been achieved previously using mechanical,¹⁴ thermal,¹⁵ or capillary forces¹⁶ to merge particles together. Here, the printed structures are inherently and highly conductive without any post-processing.

To our surprise, the resulting structures have structural anisotropy due the shear stresses from printing that align and elongate the liquid metal within the inks. The anisotropy, combined with the stress arising by rapid removal of the water from the MC by heat, causes the printed parts to change shape and thus enable four-dimensional (4D) printing of metallic structures. 4D printing is attractive because it endows static printed objects with the ability to change shape in response to stimuli such as heat, light, pH, solvent, electrical field, or magnetic field.¹⁷ The stimuli can cause shape change either by allowing relaxation of stress built into the part during fabrication (e.g., stress from polymerization) or by generating stress (e.g., thermal expansion mismatch, swelling of gels, or liquid crystal disorder).^{18,19} An effective way to precisely control the deformation of 3D structures is to print anisotropic shape-morphing filaments. Forces such as shear from dispensing²⁰ or magnetic fields²¹ can align particles in the features to program the response of the printed part to subsequent stress. Here, we print metallic gels into filamentary geometries

¹Department of Chemical and Biomolecular Engineering, North Carolina State University, Raleigh, NC 27695, USA

²School of Chemistry and Chemical Engineering, Northwestern Polytechnical University, Xi'an, Shaanxi 710072, P.R. China

³School of Chemical Engineering and Technology, Tianjin University, Tianjin 300072, P.R. China

⁴College of Computer Science and Technology, Xi'an University of Science and Technology, Xi'an, Shaanxi 710054, P.R. China

⁵College of Mechanical and Vehicle Engineering, Taiyuan University of Technology, Taiyuan, Shanxi 030024, P.R. China

⁶School of Marine Science and Technology, Tianjin University, Tianjin 300072, P.R. China

⁷Department of Electrical and Computer Engineering, National University of Singapore, 4 Engineering Drive 3, Singapore 117583, Singapore

⁸Lead contact

*Correspondence: tjuhrl@tju.edu.cn (R.H.), qiwei@tju.edu.cn (W.Q.), mddickey@ncsu.edu (M.D.D.)

<https://doi.org/10.1016/j.matt.2023.06.015>

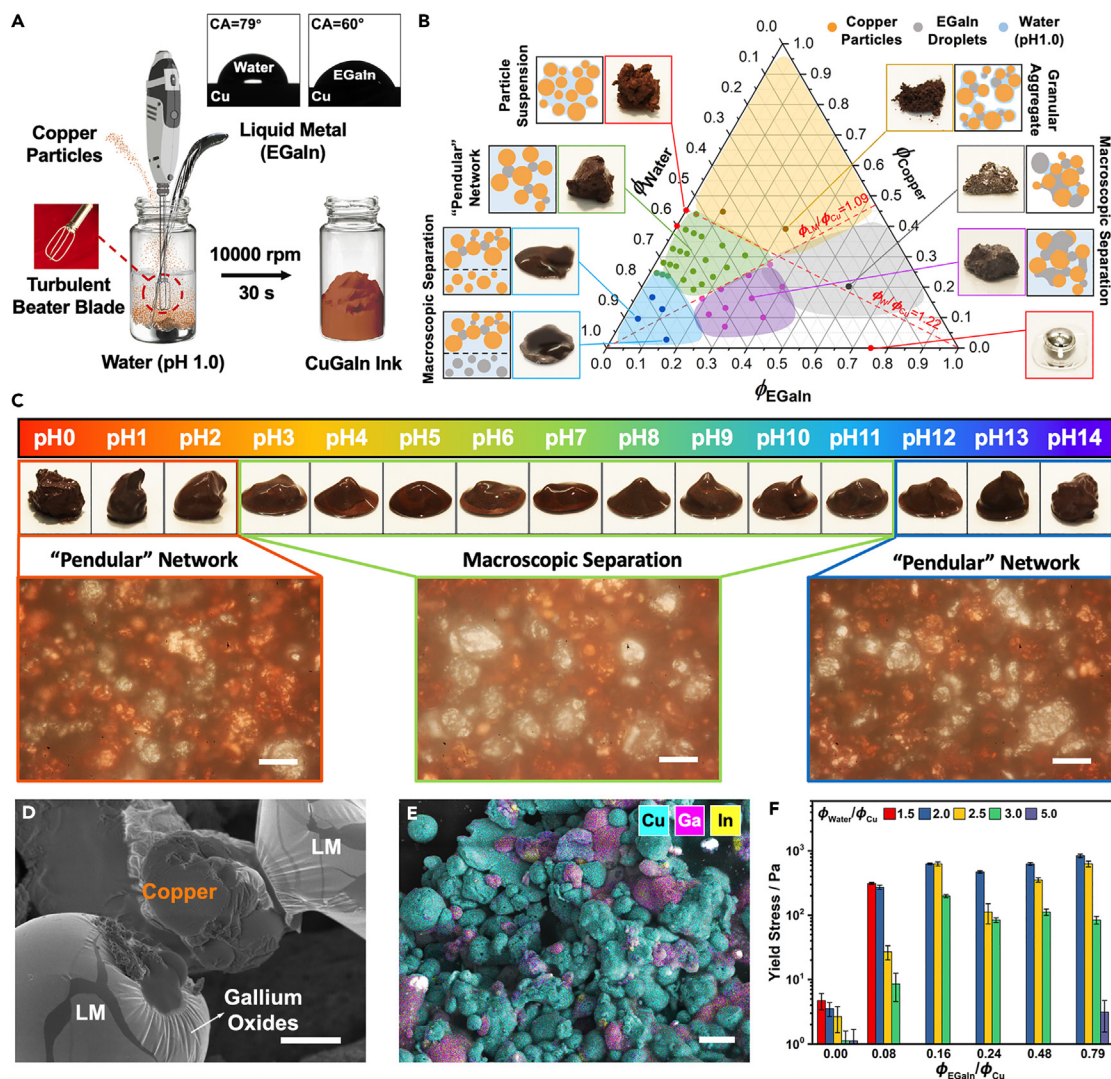


Figure 1. Cu-EGaln aqueous suspensions with different pH and compositions

(A) Schematic diagram of Cu-EGaln ink preparation and contact angle of water (in air) and EGaln (in 0.1 M HCl solution) on a flat Cu substrate. (B) Photographs of macroscopic states and morphological schematics of Cu-EGaln ternary phase diagram (pH 1). The pendular network (green data) is a metallic gel useful for printing. (C) Effects of pH value on the macroscopic states of Cu-EGaln ternary system ($S = 0.806$, $\varphi_{\text{Cu}} = 0.289$). Representative optical microscopic images of the wet suspension are shown below. Scale bars, 25 μm. (D) Close-up SEM image at the interface between Cu and EGaln particles after drying. Scale bar, 5 μm. (E) Energy-dispersive X-ray spectroscopy mapping results of samples dried at room temperature ($S = 0.806$, $\varphi_{\text{Cu}} = 0.289$). Scale bar, 25 μm. (F) Yield stress for various compositions of aqueous suspensions of Cu and EGaln (mean \pm SD).

that respond anisotropically to heat during post-processing to transform them into highly conductive 3D shapes, such as flower petals and our "Spiderbot."

RESULTS

Cu-EGaln pendular network stabilized by metallic wetting

We created wet granular suspensions by mixing Cu particles (diameter range from 10 to 25 μm) with different volumes of water and EGaln, as shown in Figure 1A. To facilitate the wetting between EGaln and Cu, we removed surface oxides by setting the pH of the water to 1.0 using HCl. After printing, the water and HCl ultimately

evaporate but initially characterize the system in the “wet” state. Following the convention of S-L-L systems, the “saturation” S characterizes the relative amount of the major liquid phase (i.e., water) in each sample in which V is the volume:

$$S = \frac{V_{\text{water}}}{V_{\text{EGaIn}} + V_{\text{water}}}.$$
 (Equation 1)

First, we consider the case of Cu particles in water, in which case $S = 1$. When the volume fraction of Cu (φ_{Cu}) exceeds 0.45 (Figure 1B), the mixture becomes granular. However, as φ_{Cu} falls below 0.40, the extra water increases the separation distance between Cu particles, thus forming a liquidous dispersion that can easily settle after mixing (Figure S1A).

Adding a small fraction of a second immiscible liquid (here, liquid metal) can significantly increase the interactions between the solid particles.⁵ This increase arises because (1) the second fluid forms bridging networks between the solid particles and (2) the addition of a second liquid makes it possible to increase the total volume fraction of the dispersed phase (which can be either liquid or solid in principle, but is solid Cu in this study). Both of these properties are important in this work because they allow us to create pastes with high loadings of metals with gel-like rheological properties suitable for printing.

We chose EGaIn as the second liquid in a system of Cu and water because EGaIn has an enormous surface tension (624 mN/m)²² and wets Cu (Figure 1A). When a small fraction of EGaIn is added ($S = 0.990$, $\varphi_{\text{Cu}} = 0.40$), the mixture forms a gel similar to conventional capillary suspensions.⁵ During mixing, the shear force applied from the beater blade and Cu particles breaks the EGaIn into droplets. The liquid metal helps bridge the Cu particles; X-ray diffraction measurements of dried samples show the presence of CuGa₂ intermetallic compound, which indicates metallic contact between Cu and EGaIn (Figure S2).²³ Interestingly, optical micrographs reveal that the EGaIn droplets are larger (25 μm) than the Cu particles (10 μm), which is atypical for S-L-L capillary systems (Figure S3).

Since the interfacial metallic wetting is the key to forming such a gel-like suspension system, the almost instant formation of the gallium oxide layer can be a barrier that limits the effective wetting between EGaIn and Cu. The oxide layer of EGaIn is amphoteric and can be removed by either acid or base.²⁴ To investigate the influence of pH on the contact state between EGaIn and Cu particles for $S = 0.806$ and $\varphi_{\text{Cu}} = 0.289$, a survey of solution pH from 1 to 14 is presented (Figure 1C). For pH between approximately 3 and 11, the passivating oxide layer of EGaIn is stable.²⁵ In this pH range, Cu-EGaIn metal particles macroscopically settled (apparent from the photographs in Figure 1C); this behavior is consistent with the system having insufficient liquid bridges to form a network. In contrast, S-L-L samples prepared at pH 1 or 13 show a highly elastic gel-like behavior, as apparent from the photographs in Figure 1C. The micrographs in Figure 1C are taken in the wet state, and appear to show liquid metal particles in contact with the Cu. Samples dried for scanning electron microscopy (SEM) imaging show EGaIn droplets distributed and bridged between Cu particles with no obvious coalescence (Figures 1D and 1E). Although EGaIn typically coalesces at low pH, the absence of coalescence is consistent with EGaIn wetting Cu within the crowded particle environment. We also observed an increase in pH after stirring (from pH 1 to pH ~3), which may be due to acid evaporation or consumption of H⁺.

Gallium or copper oxides can be dissolved in acidic conditions, leaving behind the corresponding chloride salts. However, since there is a limited amount of native

oxide on fresh Cu powder, the residual amount of chloride in the final dried sample is expected to be low. As evidenced by the X-ray photoelectron spectroscopy results ([Figure S4](#)), the overall Cl content on the surface of the sample after drying is less than 0.1%. Therefore, it is reasonable to assume that the chloride salts have a negligible effect on the final properties of these materials. Although Cu-EGaIn can also form a pendular suspension in alkaline solutions, the NaOH cannot evaporate after printing and can therefore greatly accelerate the corrosion of Cu in the printed parts. Therefore, we chose to focus on using an acidic Cu-EGaIn aqueous phase for the remainder of this paper.

To further explore the influence of composition on the morphology of the Cu/EGaIn/water system, we report a ternary phase diagram in [Figure 1B](#). Compared with conventional oil-water pendular network suspensions (PNS), the materials used here show a wider range of gel-like behavior (green area in [Figure 1A](#)), presumably due to the strong metallic wetting forces. The upper and bottom boundary can be roughly defined by $\varphi_{\text{EGaIn}}/\varphi_{\text{Cu}} = 1.09$ and $\varphi_{\text{Water}}/\varphi_{\text{Cu}} = 1.22$, which refers to the maximum EGaIn concentration that forms only bridges between Cu particles (without excess liquid metal) and the minimum water concentration that forms a continuous bulk phase, respectively. Beyond these two boundaries (yellow area), granular Cu aggregate forms because of insufficient EGaIn bridging and water dispersion ([Figure S1B](#)). As expected, an excessive water concentration ($\varphi_{\text{Water}} > 0.7$, blue area) creates a liquidous suspension with macroscopic separation of metallic particles from the water. This region is distinguished roughly by $\varphi_{\text{EGaIn}}/\varphi_{\text{Cu}} = 1.09$ ([Figures 1B, S1C, and S1D](#)). With a moderate water concentration ($0.4 < \varphi_{\text{Water}} < 0.7$, purple area)—though a gel-like suspension can still form—the excessive EGaIn causes coalescence and even engulfs entire Cu particles, resulting in a significant decrease in strength ([Figure S1E](#)). At a water fraction below 0.4 the material is solid-like, but coalescence of EGaIn droplets becomes so intense that even a small shear force will induce the bulk separation of EGaIn from the mixture ([Figure S1F](#)). The green-colored area depicts the window of stable Cu-EGaIn pendular suspensions (i.e., "metallic gels").

We used a rheometer to estimate the yield stress of the stable inks to identify compositions that might be suitable for printing. As expected, in the absence of EGaIn there is almost no yield stress ([Figure 1F](#)). The yield stress increases by two orders of magnitude within $\varphi_{\text{EGaIn}}/\varphi_{\text{Cu}} = 0.08$ and then gradually reaches a plateau. As expected, adding water lowers yield stress: for $\varphi_{\text{EGaIn}}/\varphi_{\text{Cu}}$ from 0 to 0.79, increases in $\varphi_{\text{Water}}/\varphi_{\text{Cu}}$ decrease the yield stress; however, the decrease in yield stress is small when $\varphi_{\text{Water}}/\varphi_{\text{Cu}}$ is below 2.0. Moreover, with an increase in $\varphi_{\text{EGaIn}}/\varphi_{\text{Cu}}$ (beyond 0.79) the yield stress becomes less sensitive to water fraction, which may be attributed to the richer liquid metal bridging and the increase of total particle packing density. We proceeded to print samples with $\varphi_{\text{EGaIn}}/\varphi_{\text{Cu}} = 0.48$ (see [experimental procedures](#) for details and [Table S1](#) for ink formulation).

Shear-induced alignment during printing of Cu-EGaIn ink

The suspensions reported in this work show a large distance (s) separating solid particles relative to the radius (r_p) of the Cu particles, which is unconventional in normal PNS systems. In general, the capillary force of the liquidous bridge decreases when s increases and reaches a critical value (s_c) at which the bridges pinch off. Usually, $s_c < 0.5r_p$ ²⁶; however, we found in this work that s was in the range of $0.75r_p$ to $1r_p$ and showed no direct relationship with the adjacent particle size over the range studied here. Like previously reported EGaIn-cell interactions,²⁷ the oxide layer of

EGaIn—which is evident in the SEM image of [Figure 1D](#)—provides structural support that helps hold the adjacent Cu particles together in the absence of acid.

High shear forces, such as those experienced in a dispensing nozzle, help dispense the inks from a nozzle.²⁸ We found that the Cu-EGaIn pendular inks could be dispensed from large nozzles (1.5 mm diameter or larger) but that it was difficult to dispense it homogeneously from smaller nozzles. The printability was improved by introducing a small amount of polymer matrix in the water phase. MC was chosen because of its rheological thickening behavior.²⁹ MC is widely used as a binder in granular systems and can create shear-thinning inks with good thixotropic properties.³⁰ With the addition of 4 wt % MC (4% of the water phase), the yield stress of Cu-EGaIn suspension increased by an order of magnitude, indicating the strong thickening effect of MC ([Figures S5A](#) and [S5B](#)). Microscopy images also show that EGaIn droplets still form pendular bridges between the Cu particles even with MC ([Figure S6A](#)).

The as-prepared ink experiences shear-thinning behavior when extruded through nozzles and can recover its rheological properties and hold its shape after exiting the nozzle ([Figures S5C](#), [S5D](#), [S6B](#), and [S6C](#)). On the contrary, the ink without liquid metal (but with the same amount of MC, water, and Cu, i.e., “Cu ink”) shows a much weaker strength and shear recovery, which proves that the liquid metal bridges play a critical role in printability. It also implies that the MC does not interfere with the liquid metal bonding in the Cu-EGaIn pendular network. Unless otherwise noted, in the remainder of the paper the Cu-EGaIn samples contain 4 wt % MC in the water phase. A small amount of glycerol was also added as a humectant to reduce the water evaporation rate ([Figure S7A](#)) and give a wider processing window during printing.

The metal granular suspension shear aligns during printing, which to the best of our knowledge is the first report of such behavior in a granular suspension, although liquid metal particles have been previously shown to shear align in elastomeric inks.³¹ As illustrated in [Figure 2A](#), the Cu-EGaIn pendular aggregates deform under the shear force around the nozzle to create shape anisotropy along the printing direction. When viewed under a microscope, we found that particle aggregates oriented (indicated by the shape of the EGaIn). For example, in the printed NCSU pattern ([Figure 2B](#)) they align along the printing direction in the horizontal direction, vertical direction, and at corners ([Figures 2D–2F](#)). A quantitative analysis of this orientation was performed by calculating the orientation of the oval EGaIn particles in ImageJ. Compared with the manually cast sample (no shear) all the printed filaments show clear peaks at 0°, which corresponds to the printing direction. As the nozzle diameter increases this orientation also becomes less prominent due to the decrease in shear force, which is consistent with the literature ([Figure 2C](#)).²⁰

Cu-EGaIn inks are composed of aligned (anisotropic) domains within a dilute isotropic polymer matrix (MC gel). After printing, heat rapidly evaporates the water, leading to stress in the printed structures. As illustrated in [Figure 2G](#), in the absence of EGaIn, a printed structure of Cu particles contracts isotropically when heated. In contrast, the aligned Cu-EGaIn pendular networks provide structural anisotropy during contraction of the printed structure. The network hinders contraction in the transverse direction, leading to a larger contraction along the perpendicular direction ($\delta_{\perp} > \delta_{\parallel}$).

The anisotropic parameter (A , [Equation S1](#)) quantifies this shrinkage behavior, with a value closer to zero being more isotropic. As shown in [Figure 2H](#), Cu-EGaIn ink ($\varphi_{\text{Water}}/\varphi_{\text{Cu}} = 3$) undergoes significant anisotropic shrinkage with an A value of 2.04. In contrast,

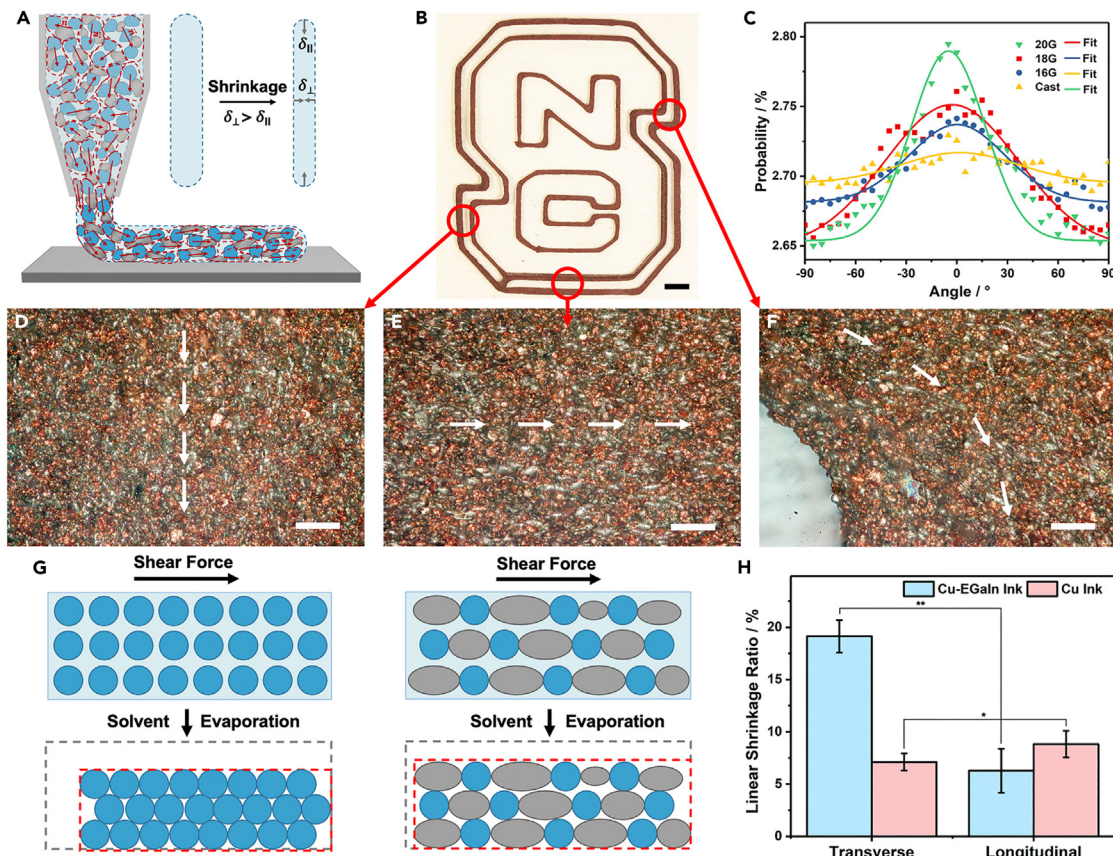


Figure 2. One-step shear alignment of Cu-EGaIn particles during printing

(A) Schematic of the shear-induced alignment of Cu-EGaIn aggregates during direct ink writing and its subsequent effect on anisotropic shrinkage ratio δ .

(B) A printed NCSU logo ($S = 0.862$, $\varphi_{\text{Cu}} = 0.223$). Scale bar, 5 mm.

(C) Quantification of the orientation using Fourier analysis: printed filaments show clear peaks at 0° , corresponding to alignment with the printing direction.

(D–F) Typical microscopy images of the printed filaments show strong orientation of Cu-EGaIn aggregates along the direction of printing. Scale bars, 100 μm .

(G) Schematic illustration of the shear-induced anisotropic shrinkage behavior of Cu ink and Cu-EGaIn ink. Blue circles denote Cu particles, and gray ellipses denote EGaIn droplets.

(H) Comparison of the anisotropic shrinkage behavior of Cu-EGaIn ink and Cu ink (mean \pm SD); * $p < 0.05$, ** $p < 0.01$.

Cu ink ($\varphi_{\text{Water}}/\varphi_{\text{Cu}} = 1.5$) exhibited almost isotropic shrinkage with an A value of 0.19. Moreover, as the nozzle size increased, the A value decreased accordingly, which indicates that this anisotropic shrinkage behavior is related to the alignment of Cu-EGaIn aggregates (Figure S8). The stronger the orientation, the larger the aspect ratio of EGaIn droplets becomes, causing more pronounced shrinkage along the transverse direction.

4D printing of Cu-EGaIn ink

Anisotropic shrinkage happens widely in natural biological tissues, such as the withering of leaves or the baking of potato chips.³² Harnessing this anisotropic shape-morphing process allows us to control the curvature in the printed structure by controlling the local strain tensor.^{33,34} Previous studies have shown that for materials with anisotropic deformation, the spatial curvature of the final structure can be precisely controlled by tailoring the angle between the printed filaments in bilayer structures, based on the anisotropic swelling stress of the material.²⁰ The Cu-EGaIn ink reported in this study is in a soft gel state during printing and becomes rigid after drying, making it difficult to evaluate its specific shrinkage stress. Thus, precise

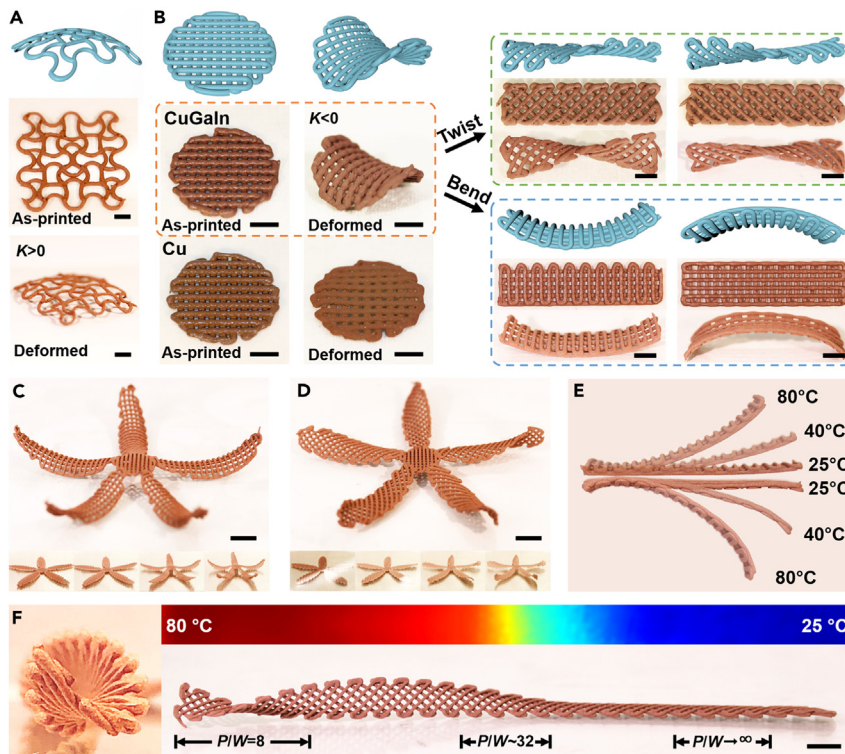


Figure 3. 4D-printed Cu-EGaIn structures with programmed curvatures

(A–D) Designed, as-printed, and dried (80°C) samples with positive (A) and negative (B) Gaussian curvature. Cu ink shrinks isotropically (no curvature) whereas Cu-EGaIn ink shows various curving behaviors due to anisotropy in the printed structure. 4D-printed flower with curling (C) and twisting (D) petal features. The insets are time-lapse captions. Scale bars, 5 mm.

(E) Effect of temperature on the deformation with either positive or negative bending directions.

(F) Programmable deformation of a twisted ribbon exposed in a temperature gradient. The degree of torsion is characterized using the ratio of pitch to ribbon width (P/W). Scale bar, 10 mm.

“inverse design” (i.e., determining *a priori* the printed shape necessary to achieve a final 3D shape) can be challenging. Nevertheless, we were able to demonstrate the 4D printing performance of the Cu-GaIn ink by applying the inks to some commonly reported designs to confirm its ability to reliably 4D-print structures.^{20,33} For example, a single-layered structure with a printed perpendicular sinusoidal pattern formed a convex surface by drying at 80°C (Figure 3A). Moreover, the curvature of a bilayer structure with printed anisotropic filaments can be precisely designed via the temperature and printing parameters.³⁵

Figure 3 presents a series of printed orthogonal patterns that exhibit different curvatures ($K > 0$ and $K < 0$) based on the orientation of the printed filaments within the part. The printed samples were dried on an 80°C hotplate to fully evaporate water. Cu-EGaIn circular samples form a saddle, whereas Cu samples exhibit planar structure with almost isotropic shrinkage. This control experiment emphasizes the importance of the liquid metal to realize anisotropy in the printed structure.

We printed features by infilling a bilayer hatch pattern (Figure 3B). The changes in the alignment of the infill pattern led to a different configuration of curvature upon heating. Printed strips bend with $0^{\circ}/90^{\circ}$ infill alignment, whereas printed strips twist with $-45^{\circ}/45^{\circ}$ infill alignment, consistent with prior reports.²⁰ Switching the

layer order yields its corresponding enantiomeric configuration. By combining printing patterns, we successfully 4D-printed flowers with either curled ([Figure 3C](#)) or twisted ([Figure 3D](#)) petals. The transformation took place within 30 min of heating, consistent with the solvent evaporation dynamics ([Video S1](#) and [Figure S7A](#)).

Interestingly, we found that the degree of deformation of Cu-EGaIn varies with different drying temperature. As shown in [Figure 3E](#), Cu-EGaIn strips with drying temperature of 80°C has almost twice the bending curvature of samples drying at 40°C, whereas samples dried at room temperature (25°C) show only slight deformation. The samples shown in [Figure 3E](#) were imaged after 1 h of drying. The curvature did not change after 9 h of drying. The drying temperature mainly affects the water evaporation rate and the internal thermal stress.³² We ruled out the possibility of thermal gradients as the source of stress, since the high metal content and, thus, thermal conductivity of Cu-EGaIn inks results in an approximately uniform internal temperature.³⁶ The equal but opposite bending of Cu-EGaIn strips ([Figure 3E](#)) further suggests negligible deformation from thermal stress gradients.

Having ruled out thermal stress as the cause of shape change, we considered the role of water evaporation. First, we measured the rate of water evaporation to ensure it increases with temperature, as expected ([Figures S7B](#) and [S7C](#)). Water evaporation can cause capillary stresses, but to a first approximation such stresses are present to the same extent regardless of how fast water evaporates. Thus, we speculated that contractile stresses associated with the drying of the MC drives shape change. MC solutions are time-dependent materials that exhibit strong rheological dependence with time.³⁷ Consequently, a lower evaporation rate may facilitate stress relaxation of the MC polymer and, in turn, reduce the shrinkage stress down to a level where deformation is no longer feasible.

It is possible to use the dependency of stress on evaporation rate to control curvature without changing the infill pattern. To illustrate this, we printed out a long strip with –45°/45° infill direction and set it on a platform with a gradient temperature distribution from 25°C to 80°C ([Figure S9](#)). The result shows that the Cu-EGaIn strip produces varying degrees of torsion with the change of temperature gradient ([Video S2](#) and [Figure 3F](#)). Furthermore, through the quantitative analysis of the pitch (P)/width (W) ratio of the helical structure, we found that when the temperature gradually increased spatially from 25°C to 80°C, the P/W value decreased to about 8, and in the temperature region around 40°C the P/W value was about four times larger than at 80°C, which is consistent with the curvature shown in [Figure 3E](#). This implies that in addition to controlling the printing layout, the printed features can also be manipulated by changing the local temperature. This could be done, in principle, by placing printed structures on surfaces with spatially controlled temperature ([Video S2](#)), using Joule heating by passing electricity through select portions of printed structures³⁶ or using light to spatially deliver heat to the printed part; such approaches could potentially endow the printed part with secondary (external) programming of shape change.

Electrical conductivity

After drying, the printed Cu-EGaIn composite has excellent electrical conductivity (σ) as high as 1.05×10^5 S/m, which is only an order of magnitude smaller than that of pure EGaIn. The conductivity increases with the EGaIn content, since it enables the formation of better percolation networks. Percolation theory fits the experimental results well:

$$\sigma = \sigma_0 (\varphi_{\text{EGaIn/Cu}} - \varphi_{\text{EGaIn/Cu,c}})^s, \quad (\text{Equation 2})$$

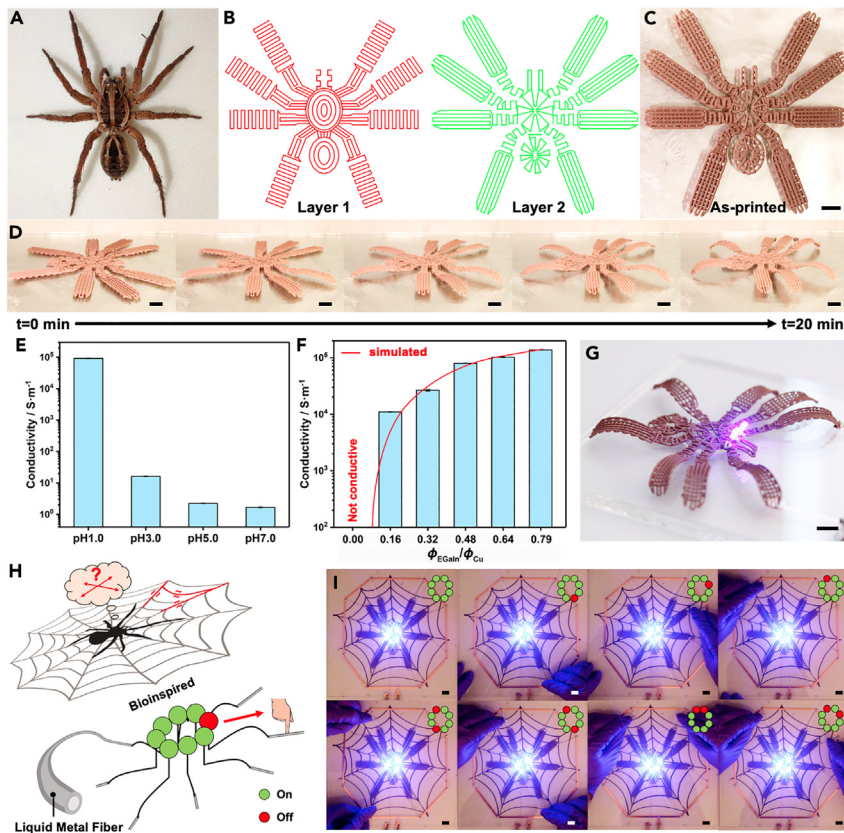


Figure 4. A complex conductive Spiderbot fabricated by 4D printing

(A) The spider architecture exhibits different configurations: positive and negative bending of legs and lifting of its own body.

(B and C) Generated printing path (B) and as-printed Spiderbot (C).

(D–F) Time-lapse photos during the thermally driven solvent evaporation process show the printed spider lifting itself up (D). Effects of solvent pH (E) and EGaN content (F) on electrical conductivity of the sample (mean \pm SD).

(G) The printed “spider robot” has excellent conductivity and can light up two LED “eyes” connected in series under 6 V DC.

(H) A bio-inspired tough sensor design: a highly stretchable EGaN fiber serves as “spider silk,” which transfers a mechanical strain variation signal to the “nervous system,” the LED arrays.

(I) Directional touch sensing via single-point touch (upper row) and dual-point touch (lower row). Scale bars, 10 mm.

where σ_0 is $2 \times 10^5 \text{ S/m}$, s is 1.44, and the critical percolation threshold $\phi_{\text{EGaN/Cu},c}$ is 0.01 according to the best fit (red plot) of conductivity data in Figure 4F. This critical value also agrees well with the observation that very little EGaN addition ($\phi_{\text{EGaN/Cu}} = 0.015$) is needed to form a pendular network (Figure S1A). The sample printed with only Cu ink is electrically insulating owing to the poor connection between the Cu particles, especially in MC solution (Figures 4F and S10).

Importantly, samples printed with Cu-EGaN inks at neutral pH were orders of magnitude less conductive ($\sim 1 \text{ S/m}$) than those printed with acidic inks. Prior studies have shown that capillary forces during drying can help “sinter” (percolate) liquid metal particles.³⁸ Here, we ruled out the possibility that capillary forces induce sintering between particles, since pH-neutral inks did not sinter during drying. Instead, it appears that acid promotes metal-metal contact to create conductive printed parts, although the stresses associated with drying likely help bring particles in better

contact ([Figure S10](#)). We note that the inks in the wet state have a conductivity of ~1 S/m regardless of pH, which suggests that networks in the wet state have only modest electrical percolation. The drying step—using the acidic inks—results in the most conductive features.

The electrical conductivity of printed Cu-EGaIn samples exhibits excellent stability at room temperature, with a variation of only 4% during the 15-day monitoring period ([Figure S11](#)). There was a slight increase in the conductivity on day 2, which presumably relates to improved contact between Ga and Cu. Additionally, we tested the stability at 80°C and found that the electrical conductivity of Cu-GaIn decreased on day 2 and eventually stabilized after 5 days. We did not observe any outwardly visible changes to the materials during aging, although we cut the samples after 15 days to investigate the cross-sections. The samples aged at elevated temperature had more pores than those at room temperature, which is consistent with the difference in conductivity. Understanding the origin of these pores is an area of ongoing work.

4D-printed Spiderbot sensor

To further demonstrate the versatility and functionality of Cu-EGaIn ink, we 4D-printed a structure that transforms to a spider shape, which we call “Spiderbot.” As shown in [Figure 4A](#), we simplify the features of spiders into two basic parts: the trunk (i.e., the head, thorax, and abdomen) and the legs. The trunk can be approximated by elliptical surfaces, and the legs can be regarded as a curved strip with opposite curvatures. Therefore, we designed the bilayer printing path as shown in [Figure 4B](#) and successfully printed the spider ([Figure 4C](#)). The as-printed structure is placed on a hotplate to induce shape deformation. With the evaporation of water, the printed “2D spider” slowly deforms and finally “lifts itself” to complete the transformation from a planar bilayer into the 3D Spiderbot ([Video S3](#) and [Figure 4D](#)). The Spiderbot has excellent conductivity and can easily light up two blue LED “eyes” connected in series under 6 V DC ([Figure 4G](#)).

Although spiders have poor eyesight and no auditory system, they can accurately and quickly judge the location of prey by the perception of leg cilia to the vibrations on the spider web.³⁹ Inspired by this property, we assembled a spider-mimicking sensing system combining the 4D-printed Spiderbot structure and a “spider web” composed of LM microfiber.⁴⁰ As illustrated in [Figure 4H](#), elastic fibers encapsulated with EGaIn were linked to each leg of the Spiderbot and LED arrays were attached in the center. This setup forms eight independent circuits between the “spider web” and the LED bulbs. When pressure is applied on the soft LM fiber, the regional strain causes an increase in resistance, which decreases the electrical voltage across the LED bulb. The decreased voltage causes the corresponding bulb to turn off. Since LED arrays are connected in parallel, the Spiderbot sensing system can also monitor the strain variation in multiple directions at the same time ([Figure 4I](#) and [Video S4](#)).

DISCUSSION

One of the key claims of this work is that it is possible to form pendular networks (gels) using conductive materials. To summarize, there are several observations that are consistent with the ink being in a pendular state. (1) Liquid metal naturally wets Cu particles in acidic conditions. (2) Microscopy images suggest that the liquid metal particles contact the Cu particles ([Figure 1C](#)). (3) Adding a small amount (~8%) of EGaIn relative to Cu results in a two-orders-of-magnitude increase in yield stress according to rheological measurements ([Figure 1F](#)). Such a large change is

consistent with network formation facilitated by liquid bridges between particles. (4) The morphology of the wet ink is pH dependent. The pendular networks appear to only form at high and low pH, where metal wetting is favorable. (5) If acid is not included during mixing, the material does not become metallically conductive after printing and drying. This latter observation rules out the possibility that capillary forces from water evaporation are causing significant percolation during drying, which has been observed in prior studies of liquid metal particles (without Cu).³⁸ The large increase in conductivity during drying of samples containing acid suggests that a more connected network is made possible by greater metal-metal contact. It is possible that capillary forces and stresses during drying help to densify pendular aggregates to facilitate percolation and thereby improve conductivity.

Conclusion and outlook

In summary, we report a metallic gel (pendular suspension) consisting of Cu particles bridged by EGaIn in acidic water. Pendular suspensions are a useful way to tune the rheology of granular suspensions by creating networks of solid particles. The novelty of this work is the use of metallic components to form the network. By varying the composition, it is possible to produce a metallic gel with a rheology that can be printed. The critical ratio of EGaIn to Cu required to achieve conductivity is low ($\phi_c = 0.01$), and the best Cu-EGaIn printed parts have an extremely high electrical conductivity (1.05×10^5 S/m). The pendular suspension is one of several morphologies that are possible by varying the relative amounts of Cu, EGaIn, and water.

By introducing a small amount of MC polymer into the pendular suspension, the Cu-EGaIn ink has desirable rheological properties for 4D printing at room temperature. Shear from printing aligns the Cu-EGaIn ink owing to the presence of the liquid metal. Consequently, when heated, the printed structures shrink anisotropically as residual water evaporates from the ink. Furthermore, the control of the printing path can program the shear alignment and, thus, curvature of the printed architecture in response to heating. The local temperature allows control over the degree of deformation to create gradient 4D-printed architectures without changing the printing pattern.

There are many ways to build on this work. We focused here on Cu particles, but the principles should extend to other metal particles or non-metallic particles coated with metal. The composition can be tuned considering the wide compositional window of printability and the ability to use a variety of particle compositions. For example, the resulting parts are solid, but it may be possible to tune the composition so the inks form parts that remain soft and gel-like. It may also be possible to calcine the samples to form new alloys, considering the high metal loading in the printed parts (up to 97.5 wt %). The current 4D printing shape change is not reversible. Thus, there are also opportunities to explore other rheological modifiers beyond MC that may add functionality, including ones that might endow reversible deformation or ones that might result in more elastic and, thus, stretchable conductors. In closing, the ability to print and 4D-print highly conductive features at room temperature (i.e., conditions compatible with other materials such as polymers and gels) should enable new opportunities for electronic, thermal, and composite devices.

EXPERIMENTAL PROCEDURES

Resource availability

Lead contact

All queries about experimental procedures can be directed to the lead contact, Michael D. Dickey (mddickey@ncsu.edu).

Materials availability

All relevant vendors and preparation procedures are included in the following section and in the [supplemental information](#).

Data and code availability

All relevant data are included in the paper and its [supplemental information](#).

Cu-EGaIn ink preparation

Cu powder (99%, 10–25 µm; Sigma-Aldrich, MO, USA), EGaIn (75.5 wt % Ga, 24.5 wt % In; Indium, NY, USA), and water (pH was tuned using either HCl or NaOH) were weighed into a 20-mL glass vial. The mixture was then dispersed using a beater blade (NTE2103; Northern Tool and Equipment, MN, USA) at 10,000 rpm for 30 s. A dark-brown gel-like suspension was then obtained. Thereafter, specific amounts of methylcellulose (1,500 cP; Sigma-Aldrich) were added and stirred for another 30 s. The resultant mixture was then quickly vacuumed to remove air bubbles. Typical formulations are listed in [Table S1](#).

Printing

The Cu-EGaIn inks were printed using a customized 3D printer composed of a 3-axis stage (Minitech Machinery, GA, USA) and a pressure controller (Ultimus V; Nordson EFD, Germany) as described previously.⁹ Inks were loaded into a 10-mL syringe barrel and degassed under vacuum before being mounted onto the printer. Printing motions were controlled via G-code file in the Mach3 software (Newfangled Solutions Software, ME, USA). Typical ink formulations are listed in [Table S1](#). The printing pressure is regulated according to the nozzle diameter. For the 16G nozzle, the pressure is 25 psi. For the 18G nozzle, the pressure is set to 35 psi. For the 20G nozzle, the pressure is 50 psi. Layer height is set to 0.6 mm with nozzle stand-off distance of 0.48 mm. The printing speed is 8 mm/s. The part was printed on a glass plate and was immediately transferred onto a pre-heated stage (25°C–80°C) for subsequent drying steps, where shape changes occurred according to different drying temperatures or printing designs.

Electrical characterization

Four-point probe resistance measurement was used to determine the electrical conductivity. Tested samples were molded into 50 mm × 3 mm × 3 mm (length × width × height) test strips, then loaded into a customized measuring mold ([Figure S12](#)); a thin layer of silver paste was applied at both ends of the test strip to improve the contact between sample and electrodes. The resistance data were collected by a source meter (2400; Keithley, OH, USA). All the samples were in triplicate, and each was measured three times.

Morphology characterization

Morphology of the printed Cu-EGaIn was observed by an optical microscope (BX-52; Olympus, PA, USA) and a scanning electron microscope (Verios 460L; FEI, OR, USA); The elemental composition was analyzed using energy-dispersive X-ray spectroscopy; X-ray diffraction (D8-focus; Bruker, Germany) was used to determine the crystalline composition of the printed Cu-EGaIn.

Rheology characterization

The printability of the Cu-EGaIn ink was characterized using a rheometer (AR-G2; TA Instruments, DE, USA), equipped with a 40-mm parallel-plate geometry. The shear-thinning property was measured using flow sweep mode. The yield stress and shear recovery tests were measured using oscillation mode at fixed frequency of 10 rad/s.

SUPPLEMENTAL INFORMATION

Supplemental information can be found online at <https://doi.org/10.1016/j.matt.2023.06.015>.

ACKNOWLEDGMENTS

The authors acknowledge support from the National Natural Science Foundation of China (grant no. 52203101) and China Scholarship Council (grant no. 201906250075). M.D.D. acknowledges support from the National Science Foundation Division of Civil, Mechanical and Manufacturing Innovation (grant no. 2032415). We also appreciate eceshi (www.eceshi.com) for coordinating the mechanical analysis.

AUTHOR CONTRIBUTIONS

Conceptualization, R.X., J.Y., and M.D.D.; methodology, R.X., J.Y., and D.Z.; investigation, R.X.; resources, T.V.N., M.W., and W.G.; writing – original draft, R.X.; writing – review & editing, R.H., J.K., and M.D.D.; funding acquisition, W.Q. and M.D.D.; supervision, R.H. and M.D.D.

DECLARATION OF INTERESTS

The authors declare no competing interests.

INCLUSION AND DIVERSITY

We support inclusive, diverse, and equitable conduct of research.

Received: March 7, 2023

Revised: June 2, 2023

Accepted: June 8, 2023

Published: July 5, 2023

REFERENCES

1. Mitarai, N., and Nori, F. (2006). Wet granular materials. *Adv. Phys.* 55, 1–45.
2. Murakami, R., and Bismarck, A. (2010). Particle-stabilized materials: dry oils and (polymerized) non-aqueous foams. *Adv. Funct. Mater.* 20, 732–737.
3. Chevalier, Y., and Bolzinger, M.-A. (2013). Emulsions stabilized with solid nanoparticles: pickering emulsions. *Colloids Surf. A Physicochem. Eng. Asp.* 439, 23–34.
4. Herzog, E.M., White, K.A., Schofield, A.B., Poon, W.C.K., and Clegg, P.S. (2007). Bicontinuous emulsions stabilized solely by colloidal particles. *Nat. Mater.* 6, 966–971.
5. Koos, E., and Willenbacher, N. (2011). Capillary forces in suspension rheology. *Science* 331, 897–900.
6. Bossler, F., and Koos, E. (2016). Structure of particle networks in capillary suspensions with wetting and nonwetting fluids. *Langmuir* 32, 1489–1501.
7. Koos, E., Johannsmeier, J., Schwebler, L., and Willenbacher, N. (2012). Tuning suspension rheology using capillary forces. *Soft Matter* 8, 6620–6628.
8. Kwon, J., DelRe, C., Kang, P., Hall, A., Arnold, D., Jayapurna, I., Ma, L., Michalek, M., Ritchie, R.O., and Xu, T. (2022). Conductive ink with circular life cycle for printed electronics. *Adv. Mater.* 34, 2202177.
9. Ladd, C., So, J.H., Muth, J., and Dickey, M.D. (2013). 3D printing of free-standing liquid metal microstructures. *Adv. Mater.* 25, 5081–5085.
10. Daalkhaijav, U., Yirmibesoglu, O.D., Walker, S., and Mengüç, Y. (2018). Rheological modification of liquid metal for additive manufacturing of stretchable electronics. *Adv. Mater. Technol.* 3, 1700351.
11. Neumann, T.V., and Dickey, M.D. (2020). Liquid metal direct write and 3D printing: a review. *Adv. Mater. Technol.* 5, 202000070.
12. Tang, S.-Y., Tabor, C., Kalantar-Zadeh, K., and Dickey, M.D. (2021). Gallium liquid metal: the devil's elixir. *Annu. Rev. Mater. Res.* 51, 381–408.
13. Cui, Y., Liang, F., Yang, Z., Xu, S., Zhao, X., Ding, Y., Lin, Z., and Liu, J. (2018). Metallic bond-enabled wetting behavior at the liquid Ga/CuGa₂ interfaces. *ACS Appl. Mater. Interfaces* 10, 9203–9210.
14. Cruz, S., Ramón, E., Zopf, S.F., and Boley, J.W. (2023). A 3D printed liquid metal emulsion for low stress activated stretchable electronics. *J. Compos. Mater.* 57, 00219983221149255.
15. Liu, S., Yuen, M.C., White, E.L., Boley, J.W., Deng, B., Cheng, G.J., and Kramer-Bottiglio, R. (2018). Laser sintering of liquid metal nanoparticles for scalable manufacturing of soft and flexible electronics. *ACS Appl. Mater. Interfaces* 10, 28232–28241.
16. Li, X., Li, M., Xu, J., You, J., Yang, Z., and Li, C. (2019). Evaporation-induced sintering of liquid metal droplets with biological nanofibrils for flexible conductivity and responsive actuation. *Nat. Commun.* 10, 3514.
17. Wan, X., Luo, L., Liu, Y., and Leng, J. (2020). Direct ink writing based 4D printing of materials and their applications. *Adv. Sci.* 7, 2001000.
18. Peng, X., Wu, S., Sun, X., Yue, L., Montgomery, S.M., Demoly, F., Zhou, K., Zhao, R.R., and Qi, H.J. (2022). 4D printing of freestanding liquid crystal elastomers via hybrid additive manufacturing. *Adv. Mater.* 34, 2204890.
19. Roach, D.J., Sun, X., Peng, X., Demoly, F., Zhou, K., and Qi, H.J. (2022). 4D printed multifunctional composites with cooling-rate

- mediated tunable shape morphing. *Adv. Funct. Mater.* 32, 2203236.
20. Gladman, A.S., Matsumoto, E.A., Nuzzo, R.G., Mahadevan, L., and Lewis, J.A. (2016). Biomimetic 4D printing. *Nat. Mater.* 15, 413–418.
21. Kim, Y., Yuk, H., Zhao, R., Chester, S.A., and Zhao, X. (2018). Printing ferromagnetic domains for untethered fast-transforming soft materials. *Nature* 558, 274–279.
22. Zrnic, D., and Swatik, D. (1969). On the resistivity and surface tension of the eutectic alloy of gallium and indium. *Journal of the Less Common Metals* 18, 67–68.
23. Liu, S., Qu, D., McDonald, S., Gu, Q., Matsumura, S., and Nogita, K. (2020). Intermetallic formation mechanisms and properties in room-temperature Ga soldering. *J. Alloys Compd.* 826, 154221.
24. Song, M., Daniels, K.E., Kiani, A., Rashid-Nadimi, S., and Dickey, M.D. (2021). Interfacial tension modulation of liquid metal via electrochemical oxidation. *Advanced Intelligent Systems* 3, 202100024.
25. Creighton, M.A., Yuen, M.C., Morris, N.J., and Tabor, C.E. (2020). Graphene-based encapsulation of liquid metal particles. *Nanoscale* 12, 23995–24005.
26. Herminghaus *, S. (2005). Dynamics of wet granular matter. *Adv. Phys.* 54, 221–261.
27. Cheeseman, S., Elbourne, A., Gangadoo, S., Shaw, Z.L., Bryant, S.J., Syed, N., Dickey, M.D., Higgins, M.J., Vasilev, K., McConville, C.F., et al. (2022). Interactions between liquid metal droplets and bacterial, fungal, and mammalian cells. *Adv. Mater. Interfaces* 9, 2102113.
28. Hao, B., Li, B., and Yu, W. (2021). Nonequilibrium structure diagram of pendular suspensions under large-amplitude oscillatory shear. *Langmuir* 37, 6208–6218.
29. Dürig, T., and Karan, K. (2019). Binders in wet granulation. In *Handbook of Pharmaceutical Wet Granulation*, S.I. Badawy and A.S. Narang, eds. (Academic Press), pp. 317–349.
30. Zhu, C., Qi, Z., Beck, V.A., Luneau, M., Lattimer, J., Chen, W., Worsley, M.A., Ye, J., Duoss, E.B., Spadaccini, C.M., et al. (2018). Toward digitally controlled catalyst architectures: hierarchical nanoporous gold via 3D printing. *Sci. Adv.* 4, eaas9459.
31. Haake, A., Tutika, R., Schloer, G.M., Bartlett, M.D., and Markvicka, E.J. (2022). On-demand programming of liquid metal-composite microstructures through direct ink write 3D printing. *Adv. Mater.* 34, 2200182.
32. Mahiuddin, M., Khan, M.I.H., Kumar, C., Rahman, M.M., and Karim, M.A. (2018). Shrinkage of food materials during drying: current status and challenges. *Compr. Rev. Food Sci. Food Saf.* 17, 1113–1126.
33. Boley, J.W., van Rees, W.M., Lissandrello, C., Horenstein, M.N., Truby, R.L., Kotikian, A., Lewis, J.A., and Mahadevan, L. (2019). Shape-shifting structured lattices via multimaterial 4D printing. *Proc. Natl. Acad. Sci. USA* 116, 20856–20862.
34. Wang, Z., Wang, Z., Zheng, Y., He, Q., Wang, Y., and Cai, S. (2020). Three-dimensional printing of functionally graded liquid crystal elastomer. *Sci. Adv.* 6, eabc0034.
35. Barnes, M., Sajadi, S.M., Parekh, S., Rahman, M.M., Ajayan, P.M., and Verduzco, R. (2020). Reactive 3D printing of shape-programmable liquid crystal elastomer actuators. *ACS Appl. Mater. Interfaces* 12, 28692–28699.
36. Jin, Y., Lin, Y., Kiani, A., Joshipura, I.D., Ge, M., and Dickey, M.D. (2019). Materials tactile logic via innervated soft thermochromic elastomers. *Nat. Commun.* 10, 4187.
37. Benchabane, A., and Bekkour, K. (2008). Rheological properties of carboxymethyl cellulose (CMC) solutions. *Colloid Polym. Sci.* 286, 1173–1180.
38. Yuen, M.C., Creighton, M.A., and Tabor, C.E. (2020). Self-sintering liquid metal colloidal inks for facile manufacture of stretchable conductors. In *2020 3rd IEEE International Conference on Soft Robotics (RoboSoft) (IEEE)*, pp. 676–681.
39. Zhang, X., Guo, J., Fu, X., Zhang, D., and Zhao, Y. (2021). Tailoring flexible arrays for artificial cilia actuators. *Advanced Intelligent Systems* 3, 202000225.
40. Zhu, S., So, J.H., Mays, R., Desai, S., Barnes, W.R., Pourdeyhimi, B., and Dickey, M.D. (2013). Ultrastretchable fibers with metallic conductivity using a liquid metal alloy core. *Adv. Funct. Mater.* 23, 2308–2314.

Supplemental information

Metallic gels for conductive 3D and 4D printing

Ruizhe Xing, Jiayi Yang, Dongguang Zhang, Wei Gong, Taylor V. Neumann, Meixiang Wang, Renliang Huang, Jie Kong, Wei Qi, and Michael D. Dickey

Table S1. Typical compositions of Cu-EGaIn inks used in this work

Copper / g	EGaIn / g	Water / g	Methyl Cellulose / mg	Glycerol / mg	Metal Content after Dying*
9	0	3 (pH1)	120	240	96.2%
9	0.5	3 (pH1)	120	240	96.3%
9	1.0	3 (pH1)	120	240	96.5%
9	2.0	3 (pH1)	120	240	96.8%
9**	3.0	3 (pH1)	120	240	97.1%
9	5.0	3 (pH1)	120	240	97.5%
9	3.0	3 (pH3)	120	240	97.1%
9	3.0	3 (pH5)	120	240	97.1%
9	3.0	3 (pH7)	120	240	97.1%

*Metal content is calculated based on weight.

** This formulation is used for all 3D printing experiments.

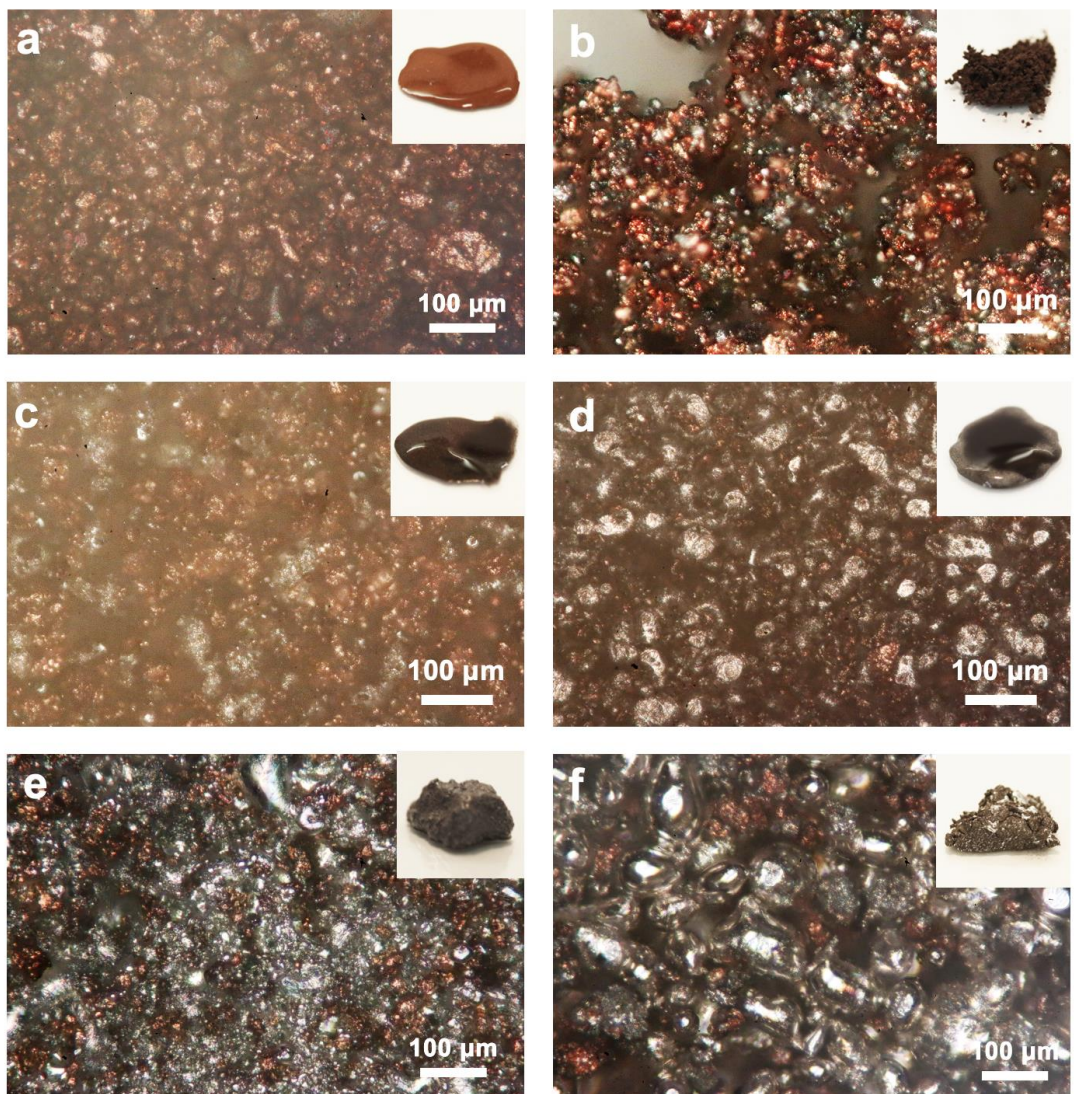


Figure S1. Macroscopic and microscopic images of typical Cu-EGaIn suspensions (shown in Figure 1b) at pH=1. **a.** $S=1.00$, $\phi_{\text{Cu}}=0.40$. **b.** $S=0.481$, $\phi_{\text{Cu}}=0.39$. **c.** $S=0.950$, $\phi_{\text{Cu}}=0.19$. **d.** $S=0.848$, $\phi_{\text{Cu}}=0.03$. **e.** $S=0.612$, $\phi_{\text{Cu}}=0.16$. **f.** $S=0.255$, $\phi_{\text{Cu}}=0.20$.

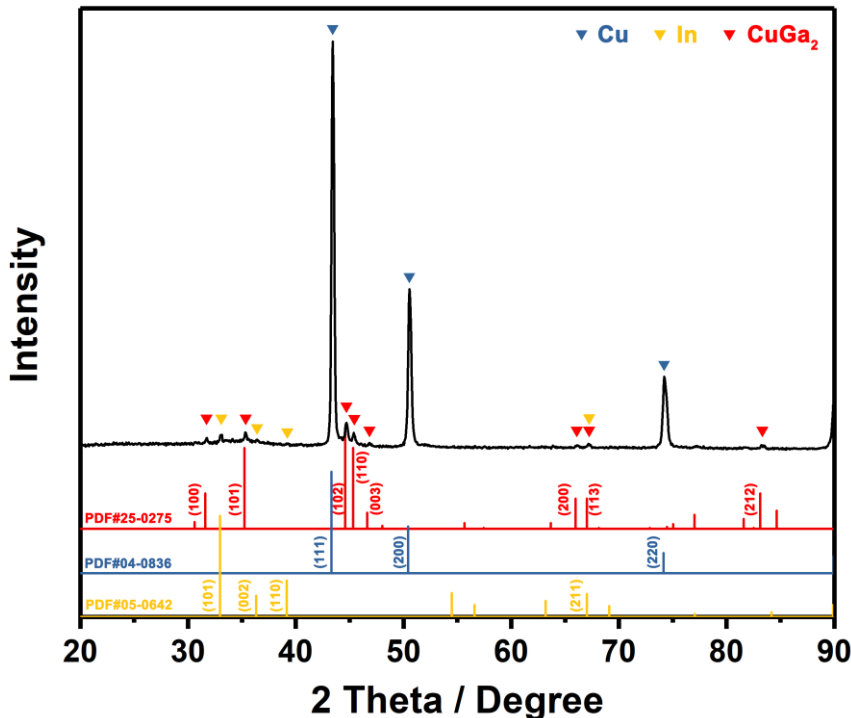


Figure S2. X-ray diffraction (XRD) pattern of the Cu-EGaIn ink ($S=0.806$, $\phi_{\text{Cu}}=0.289$, pH=1) after drying. The colored data are the standard PDF cards corresponding to the detected peaks (CuGa₂: PDF#25-0275, Cu: PDF#04-0836, In: PDF#05-0642). The peak of CuGa₂ intermetallic compound is clearly seen and denoted in red. The peaks denoted in blue attribute to the copper crystal lattice. The very weak peaks in yellow are attributed to crystalline indium, resulting from the dealloying of EGaIn at CuGa₂/Ga interface due to the local depletion of Ga from the eutectic.

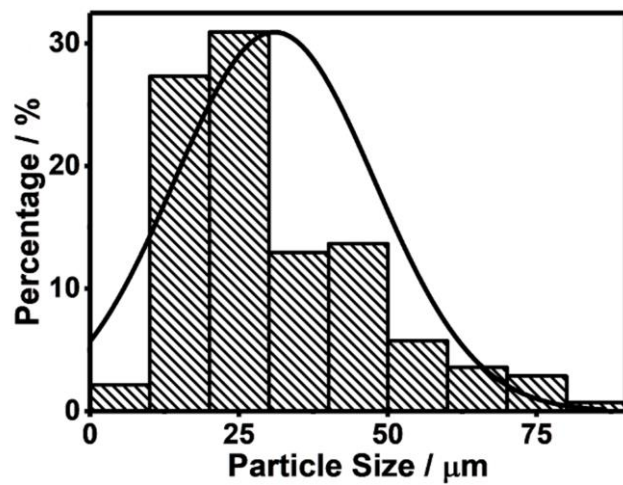


Figure S3. Size distribution curve of EGaIn droplets in Cu-EGaIn sample ($S=0.990$, $\phi_{\text{Cu}}=0.40$, pH=1.0).

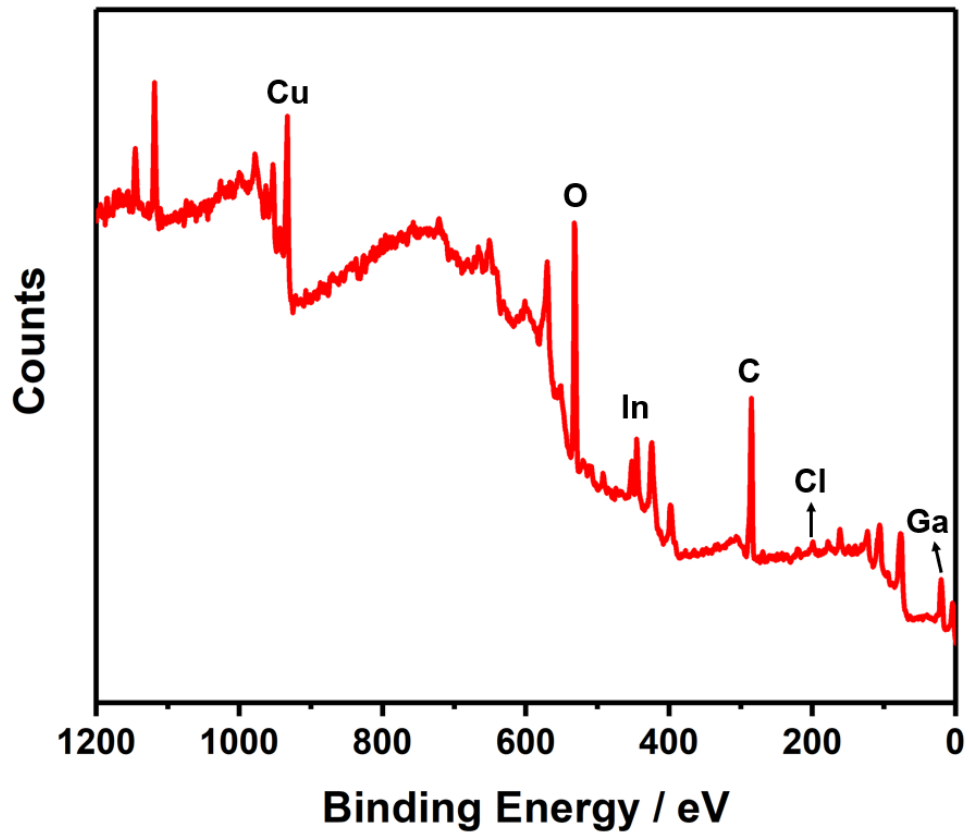


Figure S4. XPS scan of Cu-EGaIn sample (without MC) prepared at pH=1.0.

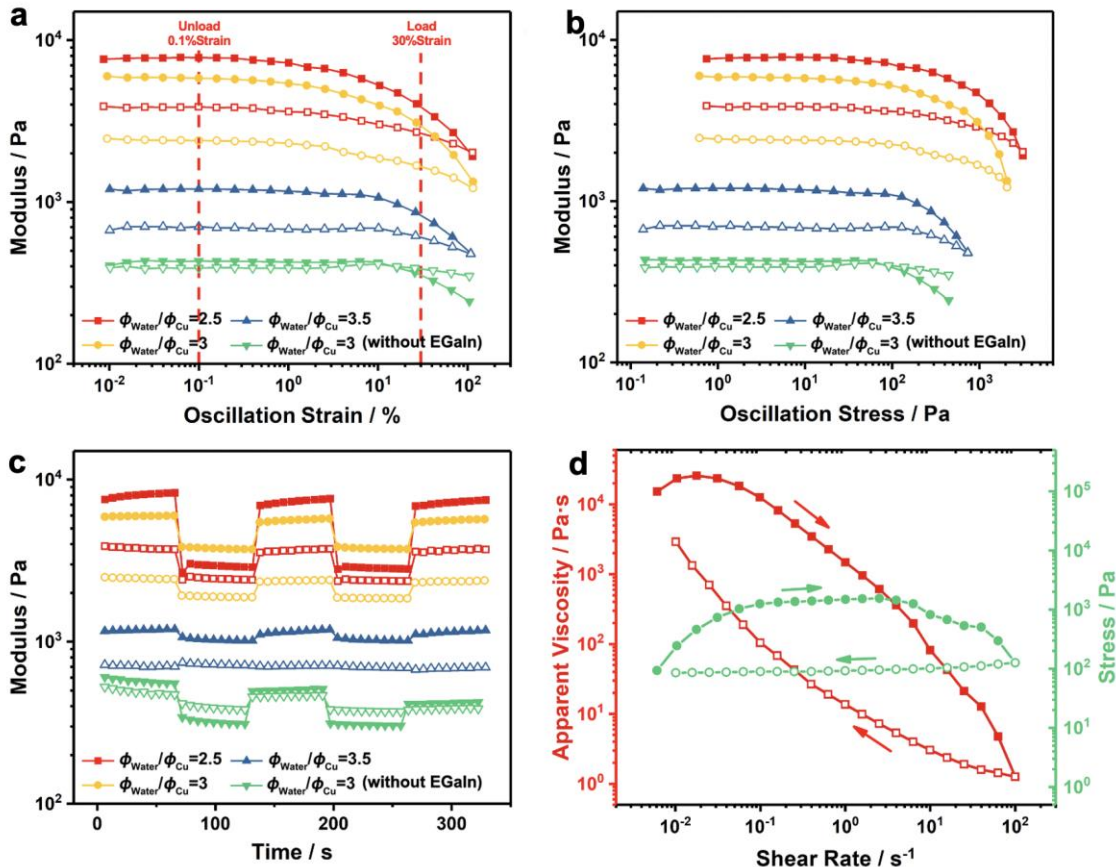


Figure S5. Rheological behavior of the as-prepared Cu-EGaIn ink (with addition of 4 wt% methylcellulose and a fixed $\phi_{\text{EGaIn}}/\phi_{\text{Cu}}=0.48$). Modulus expressed versus oscillation strain (**a**) and stress (**b**). Oscillation recovery test (**c**) is presented at an alternate high (30%) and low (0.1%) strain, which are indicated by vertical lines in **a** for convenience. **d.** Thixotropic loop test at shear rate between 0.01-100 s^{-1} ($\phi_{\text{Water}}/\phi_{\text{Cu}}=3$).

Control of ink thixotropic properties is important for reliable flow through nozzles and careful programming of shear-reversible viscoelasticity is vital for shape retention after deposition. These properties are mainly adjusted by varying the water to copper ratio ($\phi_{\text{Water}}/\phi_{\text{Cu}}$). **Figure S5a** shows the storage and loss moduli as a function of oscillation strain. Samples with higher water content have a lower plateau modulus

value whereas the sample without EGaIn has a plateau modulus one order of magnitude smaller. From **Figure S5b**, the yield stress also decreases with the increase in water content and Cu ink shows a significantly smaller yield stress (98.7 Pa) than Cu-EGaIn inks (2135 Pa). **Figure S5c** depicts variation of storage and loss moduli when applying alternate high (30%) and low (0.1%) strain. Samples containing 4wt% MC can be restored to the modulus of the previous state when the strain alters. Cu inks have a modulus that gradually decreases because of its weak particle interconnection. Plus, Cu-EGaIn inks show an almost overlapping trace by cycling shear (**Figure S5d**), which indicates that Cu-EGaIn ink ($\phi_{\text{Water}}/\phi_{\text{Cu}}=3$) can recover its strength and can hold its shape right after being extruded through the printing nozzle. However, Cu inks shows a poor rheological property in the same water to copper fraction, therefore $\phi_{\text{Water}}/\phi_{\text{Cu}}$ was further reduced to 1.5 for Cu inks to achieve successful printing.

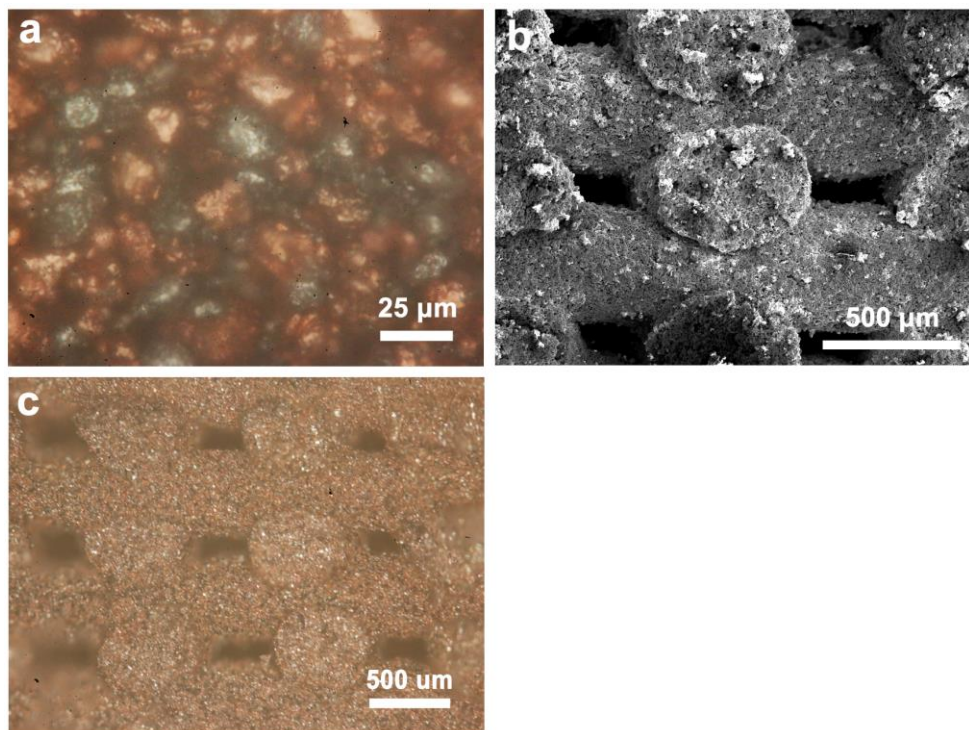


Figure S6. **a.** Microscopic image of as-prepared Cu-EGaIn ink ($\phi_{\text{Water}}/\phi_{\text{Cu}}=3$, $\phi_{\text{EGaIn}}/\phi_{\text{Cu}}=0.48$, 4% MC at pH=1.0). **b-c.** SEM and microscopic images of the as-printed CuGaIn woodpile scaffold.

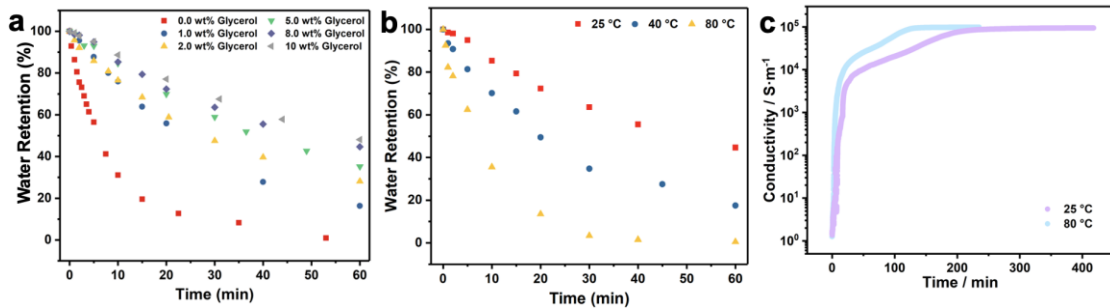


Figure S7. **a.** The effect of glycerol content on evaporation rates at 25 °C. A small addition of glycerol noticeably decreases the evaporation rate. **b.** The effect of temperature on the water retention as a function of time to quantify the rate of evaporation. Samples dried at 80 °C has almost twice the evaporation rate as that at 25 °C within 60 min. **c.** The effect of evaporation temperature on the conductivity evolution. The evolution of conductivity is divided into three stages: As depicted in Figure S9c, within the first 30 min, the conductivity quickly increased by 4 orders of magnitude due to the shrinkage of polymer matrix, which further facilitate the formation of new Cu-EGaIn bridges. After 30 min, the evaporation rate slows down, causing the shrinkage rate decreases significantly. At about 140 min, the conductivity reaches a plateau where the drying temperature does not influence the plateau conductivity.

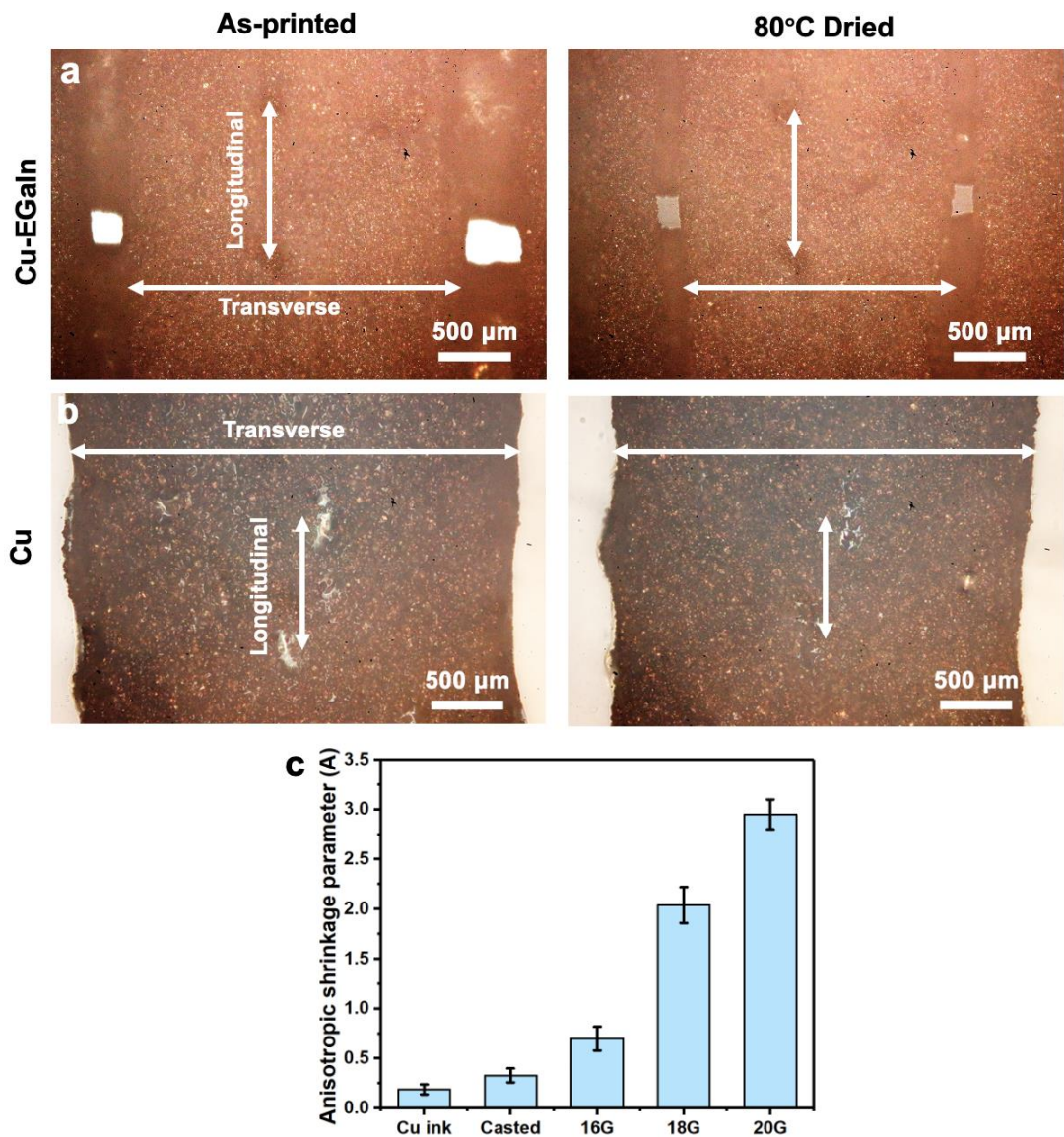


Figure S8. Comparison of linear shrinkage ratio under microscope of **a.** CuGaIn ink ($\phi_{\text{Water}}/\phi_{\text{Cu}}=3$, $\phi_{\text{EGaIn}}/\phi_{\text{Cu}}=0.48$, 4% MC at pH1) and **b.** Cu ink ($\phi_{\text{Water}}/\phi_{\text{Cu}}=1.5$, 4% MC at pH1). The Cu-EGaIn ink shows a noticeable higher shrinkage ratio along longitudinal direction whereas Cu ink almost shows an isotropic shrinkage. **c.** depicts the influence of nozzle size on the A value.

The anisotropic shrinkage parameter (A) is calculated using the below equation:

$$A = \left| \frac{\delta_{\perp}}{\delta_{\parallel}} - 1 \right| \quad \text{S1}$$

Where δ_{\perp} and δ_{\parallel} are the linear shrinkage ratio (L/L_0) along the transverse and longitudinal direction respectively (L_0 is the original length right after printing).

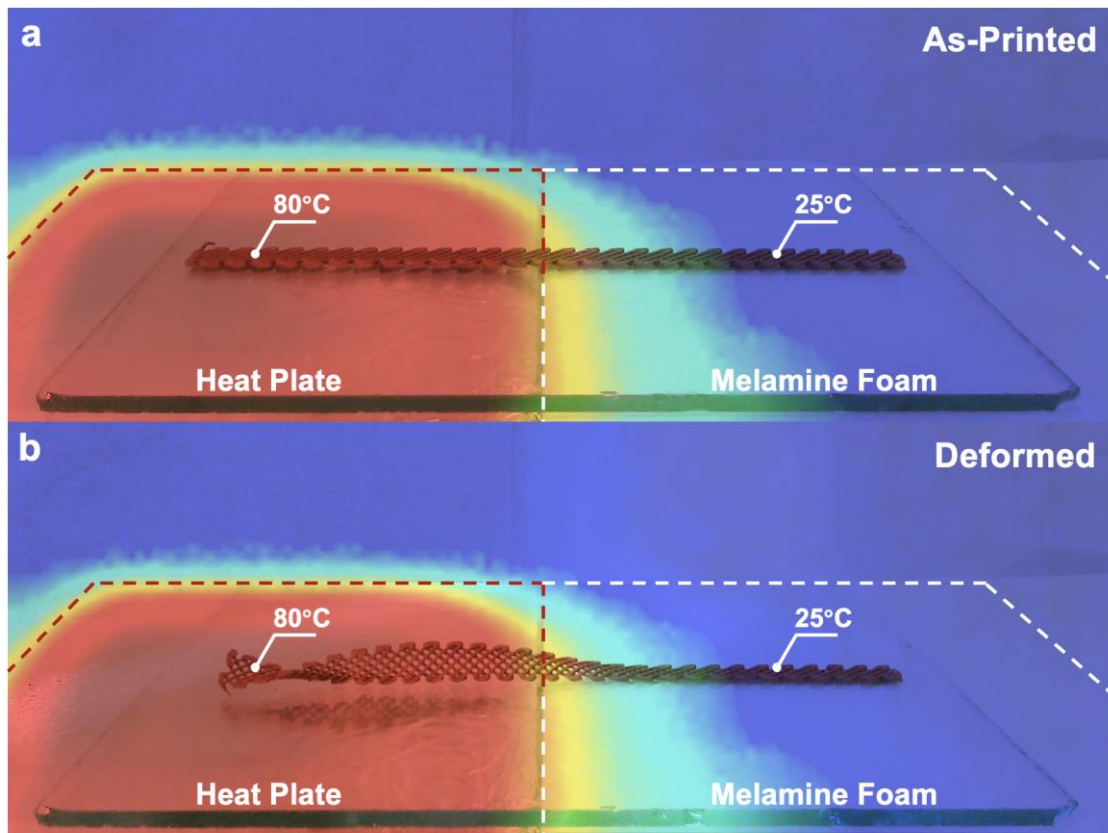


Figure S9. Experiment apparatus of temperature-controlled deformation. **a.** as printed Cu-EGaIn strip and **b.** after dried on a temperature gradient surface. The temperature gradient surface is realized by setting a hot plate and a Melamine Foam (serves as heat barrier) side by side. The melamine foam provides excellent thermal insulation and can still maintain 25 °C when the hot plate is set to 80 °C. The real temperature distribution is visualized by an IR camera where the temperature at center of the sample is around 40 °C.

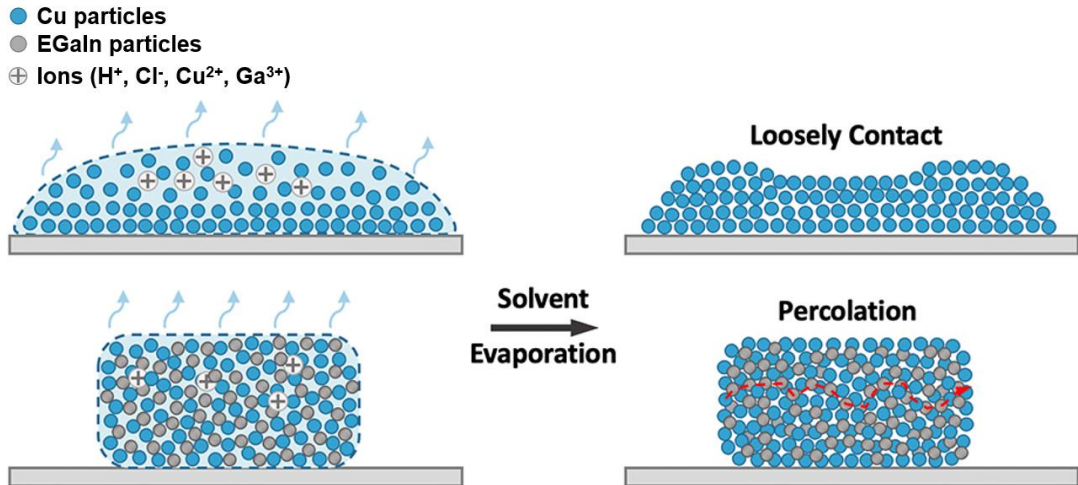


Figure S10. Schematic illustration of conductive path formation in Cu ink and CuGaIn ink during solvent evaporation. As water evaporates, the MC gel shrinks, which causes more Cu-EGaIn aggregates to come into contact (bottom row), therefore making a percolation path throughout the sample. In absence of EGaIn (top row of the image), the copper particles cannot form effective percolation due to the barrier of MC layer.

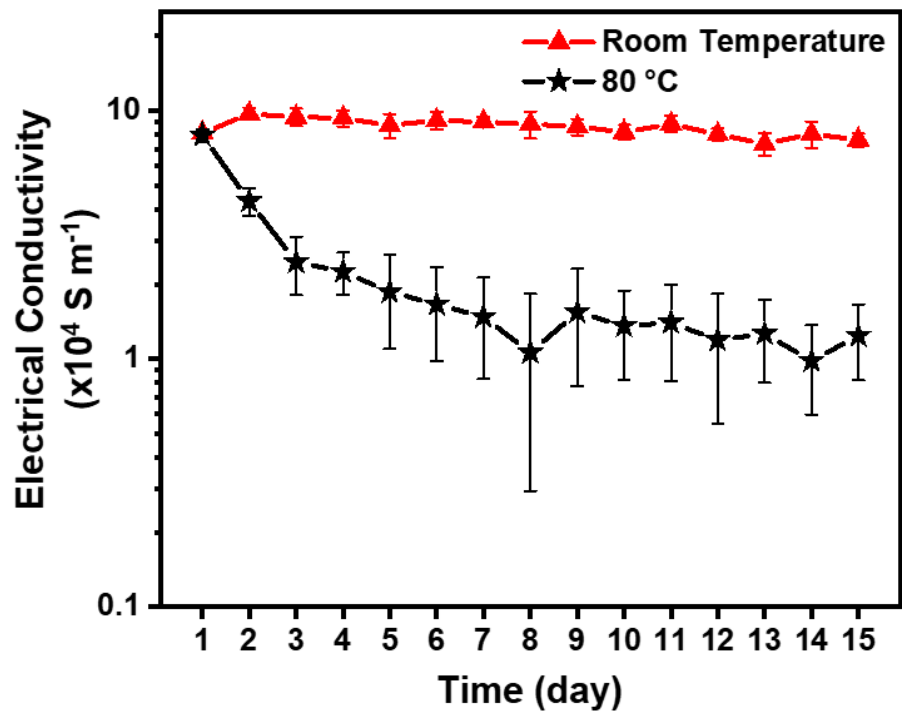


Figure S11. Electrical conductivity stability over 15 days at room temperature or 80 °C oven.

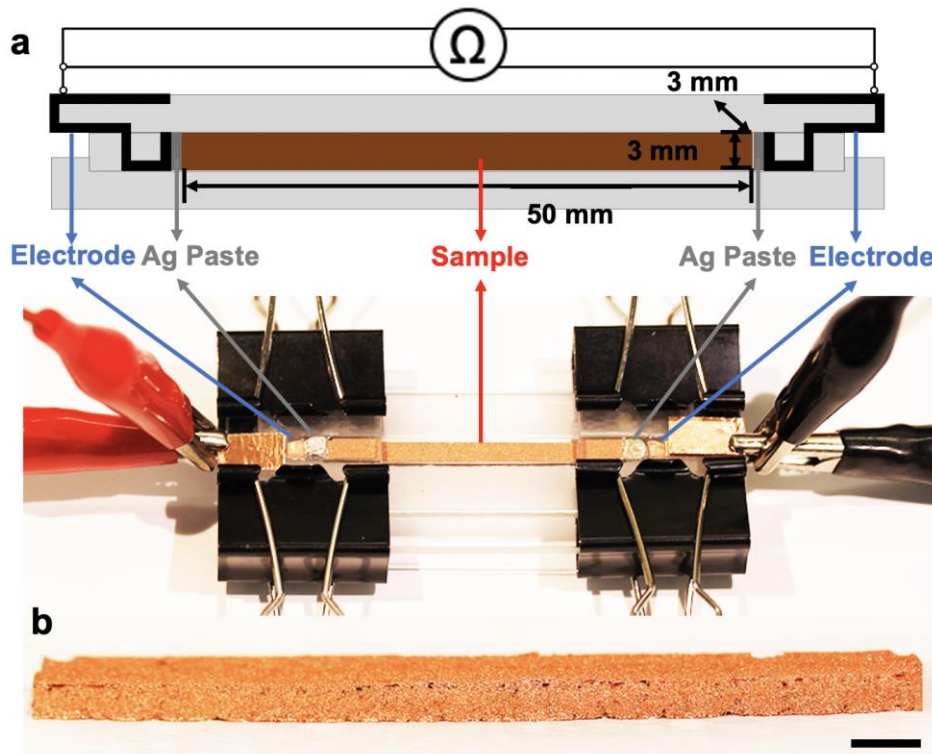


Figure S12. **a** Schematic and photography of the electrical conductivity test apparatus.

b is the $50 \times 3 \times 3$ mm test strip after drying at ambient condition overnight. (Scale bar: 5 mm)

The electrical conductivity (σ) was calculated using the following equation:

$$\sigma = \frac{L}{R \cdot S} \quad \text{S2}$$

Where L is length of the test strip, S is the cross-sectional area of the test strip, and R is tested resistance.